

# Spatial Privacy-aware VR streaming

Xing Wei and Chenyang Yang

School of Electronics and Information Engineering, Beihang University, Beijing 100191, China

Email: {weixing, cyyang}@buaa.edu.cn

**Abstract**—Proactive tile-based virtual reality (VR) video streaming employs the current tracking data of a user to predict future requested tiles, then renders and delivers the predicted tiles to be requested before playback. Very recently, privacy protection in VR video streaming starts to raise concerns. However, existing privacy protection may fail even with federated learning at head mounted display (HMD). This is because when the HMD requests the predicted requested tiles and the prediction is accurate, the real requested tiles and corresponding user behavior-related data can still be recovered at multi-access edge computing server. In this paper, we consider how to protect privacy even with accurate predictors and investigate the impact of privacy requirement on the quality of experience (QoE). To this end, we first add extra *camouflaged* tile requests in addition to real tile requests and model the privacy requirement as the *spatial degree of privacy* (sDoP). By ensuring sDoP, the real tile requests can be hidden and privacy can be protected. Then, we jointly optimize the durations for prediction, computing, and transmitting, aimed at maximizing the privacy-aware QoE given arbitrary predictor and configured resources. From the obtained optimal closed-form solution, we find that the increase of sDoP improves the capability of communication and computing hence improves QoE, but degrades the prediction performance hence degrades the QoE. The overall impact depends on which factor dominates the QoE. Simulation with two predictors on a real dataset verifies the analysis and shows that the overall impact of sDoP is to improve the QoE.

**Index Terms**—privacy-aware VR, proactive VR, privacy protection, spatial degree of privacy

## I. INTRODUCTION

Wireless virtual reality (VR) can provide a seamless and immersive experience to users. As the main type of VR services, 360° video has the following unique features. First, 360° video usually has 360° × 180° panoramic view with ultra high resolution (e.g., binocular 16K [1]). Second, the range of angles of a 360° video that humans can see at arbitrary time is only a small portion of the full panoramic view (e.g., 110° × 90°), which is called field of view (FoV). Third, the stalls or black holes during watching 360° video will cause physiological discomfort, e.g., dizziness, which degrades the quality of experience (QoE) and thus should be avoided.

To stream such video with QoE guarantee, proactive VR video streaming is proposed [2], which divides a full panoramic view segment into small tiles in spatial domain. Before the playback of the segment, the tiles to be most likely requested in the segment are first predicted using the user behavior-related data in an observation window, which are then rendered and finally delivered to the user.

While proactive VR video streaming is being intensively investigated in academia and industry, most of the existing works neglect the willingness of users. *Are users willing to share their behavior-related data while watching 360° videos?*

Recent work shows that with less than 5 minutes tracking data while watching VR videos, random forest algorithm can correctly identify 95% of users among all the 511 users [3]. This indicates that behavior-related data can be used to infer personal information. With the development of technology, one may be able to dig more personal information than beyond imagination. Very recently, the first privacy requirement dataset shows that the privacy requirements of 360° videos among videos and users are heterogeneous and only 41% of the totally watched videos have no privacy requirement [4].

With these findings, privacy protection in VR video streaming starts to raise concerns. A privacy-preserve approach has been proposed to upload one of the user-behavior related data—eye-tracking data [5]. Privacy requirement has been defined in temporal domain and the corresponding impact on QoE has been investigated [4]. However, proactive VR streaming still needs to predict the future requested tiles. When the prediction is accurate, the user behavior-related data can still be recovered, and the privacy protection may fail. Then, here comes two problems: *How to protect privacy in VR video streaming even with accurate predictors? What is the impact of privacy protection on the system?*

In this paper, we strive to answer these questions. Our contributions can be summarized as follows.

- To protect privacy even with accurate predictors, we blur the real tile requests by adding extra *camouflaged* tile requests. Specifically, we define the spatial degree of privacy (sDoP) as a metric related to the number of extra camouflaged requested tiles in addition to real requested tiles. Then, the input of the predictor becomes a mixture of real and camouflaged requested tiles. A larger sDoP indicates more extra camouflaged tile requests, which will degrade the prediction accuracy. By introducing sDoP into QoE and ensuring that sDoP can be satisfied, the real tile requests can be efficiently hidden and privacy can be efficiently protected.
- Based on the defined privacy requirement, we optimize the durations for prediction, communication, and computing under arbitrarily given predictor as well as communication and computing resources to maximize the QoE.
- From the obtained optimal solution, we find that the increase of sDoP on the one hand improves the capability of communication and computing hence improves QoE. On the other hand, it degrades the prediction performance hence degrades the QoE. The overall impact depends on which factor dominates the QoE.
- Simulation with two predictors on a real dataset verifies the analysis and shows that the overall impact of increasing the sDoP is to improve the QoE.

## II. SYSTEM MODEL

Consider a tile-based VR video streaming system with a multi-access edge computing (MEC) server co-located with a base station (BS) that serves  $K$  users. The MEC server equips with powerful computing units for rendering and training predictors, accesses a VR video library by local caching or high-speed backhaul, thus the delay from the Internet to the MEC server can be omitted. Each user requests  $360^\circ$  videos from the library according to their own interests. Therefore, the requests can be considered different, which then can be decoupled into multiple individual requests. In the sequel, without loss of generality, we consider arbitrary one request for  $v$ th video from  $k$ th user for analysis.

The playback duration of VR video is  $T_{VR}$ . Each VR video consists of  $L$  segments in temporal domain, and each segment consists of  $M$  tiles in spatial domain. The playback duration of each tile equals to the playback duration of a segment, denoted by  $T_{seg}$  [2], [6].

Each user is equipped with an head mounted display (HMD), which can measure user behavior-related data (e.g., the head movement trace), send the tile requests to the MEC server, and pre-buffer segments. To protect the privacy of users, the HMD is also equipped with a light-weighted computing unit for training a predictor and predicting tile requests.

### A. Spatial Degree of Privacy

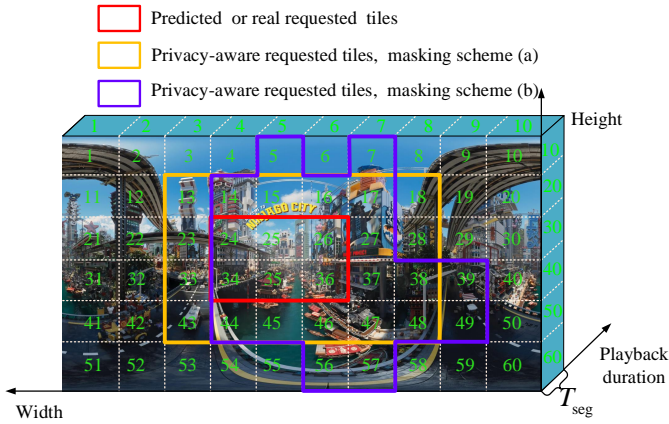


Fig. 1: Predicted or real requested tiles and privacy-aware requested tiles in a segment,  $M = 60$ ,  $N_{fov} = 3 \times 2 = 6$ ,  $N_p = 6 \times 4 = 24$ .

For training the tile request predictor or predicting the requested tiles at the MEC server by centralized learning, the requested tiles should be uploaded to the MEC server. To hide the real tile requests when a user has privacy requirement, the HMD should request a mixture of real and camouflaged requested tiles. For training at HMDs, say by federated learning, the real tile requests are only stored at the local HMD. However, when predicting at HMD, the predicted tile requests still need to be uploaded to the MEC server. When the prediction is accurate, the MEC server can obtain the spatial location of requested tiles. That is to say, *even with federated learning for VR streaming, privacy will still be leaked out*. Therefore, for the same reason of privacy

protection, the HMD should also request a mixture of real and camouflaged requested tiles. To reflect the privacy requirement in centralized and federated prediction when watching  $360^\circ$  videos, we define the *spatial degree of privacy* as the ratio of extra camouflaged requested tiles in addition to tiles in a FoV among all the extra tiles in addition to tiles in a FoV, i.e.,

$$\rho_s \triangleq \frac{N_p - N_{fov}}{M - N_{fov}} \in [0, 100\%] \quad (1)$$

where  $N_p$  is the number of privacy-aware requested tiles in a segment, which contains real and camouflaged requested tiles,  $N_{fov}$  is the number of tiles in a FoV in a segment with  $N_p \geq N_{fov}$ . Both numbers of real and predicted requested tiles are  $N_{fov}$ . To illustrate the sDoP, we provide an example in Fig. 1. The number of tiles in a FoV is  $N_{fov} = 6$ , the predicted or real requested tiles in the FoV are No. 24-26, 34-36. To protect the privacy, various masking schemes can be employed. For example, for masking scheme (a), the extra camouflaged requested tiles in addition to tiles in a FoV are No. 13-18, 23, 27, 28, 33, 37, 38, 43-48, and the number of privacy-aware requested tiles is  $N_p = 24$ . Then, sDoP is  $\rho_s = \frac{24-6}{60-6} = 33.3\%$ .

When given sDoP, the number of privacy-aware requested tiles can be obtained from (1) as

$$N_p(\rho_s) = N_{fov} + \rho_s(M - N_{fov}) \quad (2)$$

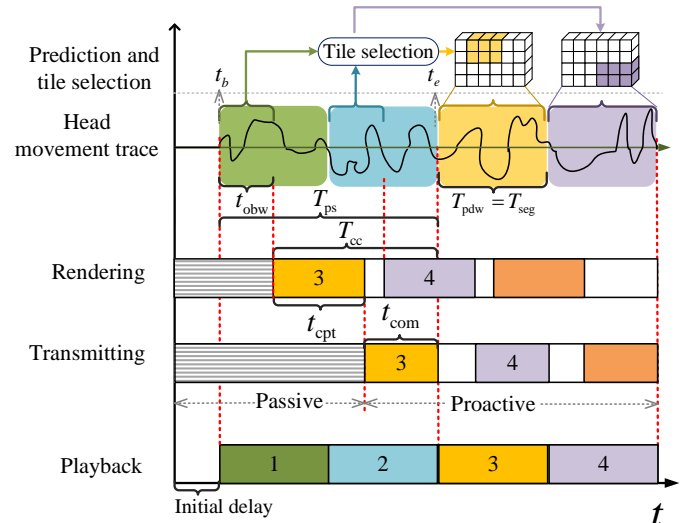


Fig. 2: Streaming the first four segments of a VR video.  $t_b$  is the start time of the observation window,  $t_e$  is the start time of playback of the  $l_0$ th segment.

### B. Streaming Procedure

As shown in Fig. 2, when a user requests a VR video with sDoP  $\rho_s$ , the MEC server first streams the initial  $(l_0 - 1)$ th segments in a passive streaming mode [7]. After an initial delay, the first segment begins to play at the time instant  $t_b$ , which is also the start time of the observation window. Then, proactive streaming for  $l_0$ th segment begins, subsequent segments are predicted, computed, and transmitted. In the sequel, we take the  $l_0$ th segment as an example for elaboration.

After the MEC server collects the user behaviour-related data in an observation windows with duration  $t_{obw}$ , the tiles

to be played in the  $l_0$ th segment with duration  $T_{\text{pdw}} = T_{\text{seg}}$  can be predicted. To avoid playback stalling, rendering and transmitting the tiles in  $l_0$ th segment should be finished before the start time of playback of  $l_0$ th segment, i.e., the time instant  $t_e$ . The duration beginning from  $t_b$  and terminating at  $t_e$ , is the proactive streaming time for a segment  $T_{\text{ps}}$ . We can observe that  $T_{\text{ps}} = (l_0 - 1)T_{\text{seg}}$ . In the figure, we consider predicting the third segment as an example, i.e.,  $l_0 = 3$ ,  $T_{\text{ps}} = 2T_{\text{seg}}$ .

Specifically, at the end of the observation window, tile request probabilities or the fixation sequences of FoVs in the  $l_0$ th segment can be predicted at HMD. Based on the probabilities (or the fixation sequences) and the number of tiles in a FoV  $N_{\text{fov}}$ , the predicted requested tiles can be obtained [4]. Given sDoP  $\rho_s$ , the number of privacy-aware requested tiles  $N_p(\rho_s)$  can be obtained from (2). Then, based on the predicted requested tiles  $N_p(\rho_s)$ , the masking scheme (say (b) in the Fig. 1), the privacy-aware requested tiles can be determined. The selected tiles are rendered with duration  $t_{\text{cpt}}$  and the sequence of FoVs can be generated, and finally the sequence of FoVs are transmitted with duration  $t_{\text{com}}$ , which should be finished before the start time of playback for the predicted segment. The durations for observation, computing, and transmitting should satisfy  $t_{\text{obw}} + t_{\text{cpt}} + t_{\text{com}} = T_{\text{ps}}$ . The duration for communication and computing can be expressed as  $t_{\text{cc}} \triangleq t_{\text{com}} + t_{\text{cpt}}$ .

### C. Computing and Transmission Model

According to the computing model in [8], the number of bits that can be rendered per second, referred to as the *computing rate*, is  $C_{\text{cpt},k} \triangleq \frac{F_{\text{cpt},k}}{\mu_r}$  (in bit/s), where  $\mu_r$  is the required floating-point operations (FLOPs) for rendering one bit of FoV in FLOPs/bit [8].

The BS serves the  $k$ th single-antenna user using zero-forcing beamforming with  $N_t$  antennas. The instantaneous data rate at the  $i$ th time slot for the  $k$ th user is

$$C_{\text{com},k}^i = B_k \log_2 \left( 1 + \frac{p_k^i d_k^{-\alpha} |\tilde{h}_k^i|^2}{\sigma^2} \right)$$

where  $B_k$  is the configured bandwidth for the  $k$ th user,  $\tilde{h}_k^i \triangleq (\mathbf{h}_k^i)^H \mathbf{w}_k^i$  is the equivalent channel gain,  $p_k^i$  and  $\mathbf{w}_k^i$  are respectively the transmit power and beamforming vector for the  $k$ th user,  $d_k$  and  $\mathbf{h}_k^i \in \mathbb{C}^{N_t}$  are respectively the distance and the small scale channel vector from the BS to the  $k$ th user,  $\alpha$  is the path-loss exponent,  $\sigma^2$  is the noise power, and  $(\cdot)^H$  denotes conjugate transpose.

We consider indoor users as in the literature, where the distances of users,  $d_k$ , usually change slightly [6], [9], [10] and hence are assumed fixed. Due to the head movement and the variation of the environment, small-scale channels are time-varying, which are assumed as remaining constant in each time slot with duration  $\Delta T$  and changing independently with identical distribution among time slots. With the proactive transmission, the rendered tiles in a segment should be transmitted with duration  $t_{\text{com}}$ . The number of bits transmitted with  $t_{\text{com}}$  can be expressed as  $\bar{C}_{\text{com},k} \cdot t_{\text{com}}$ , where

$$\bar{C}_{\text{com},k} \triangleq \frac{1}{N_s} \sum_{i=1}^{N_s} C_{\text{com},k}^i \cdot \Delta T$$

is the time average transmission rate, and  $N_s$  is the number of time slots in  $t_{\text{com}}$ . Since future channels are unknown when making the optimization, we use ensemble-average rate  $\mathbb{E}_h\{C_{\text{com},k}\}$  [11] to approximate the time-average rate  $\bar{C}_{\text{com},k}$ , where  $\mathbb{E}_h\{\cdot\}$  is the expectation over  $h$ , which can be very accurate when  $N_s$  or  $N_t/K$  is large [8].

To ensure fairness among users in terms of QoE, the transmit power is allocated to compensate the path loss, i.e.,  $p_k^i = \frac{\beta}{d_k^\alpha}$ , where  $\beta$  can be obtained from  $\beta(\sum_{k=1}^K \frac{1}{d_k^\alpha}) = P$  and  $P$  is the maximal transmit power of the BS. Then, the ensemble-average transmission rate for each user is equal.

In the sequel, we consider arbitrary one user and use  $C_{\text{com}}$  and  $C_{\text{cpt}}$  to replace  $\mathbb{E}_h\{C_{\text{com},k}\}$  and  $C_{\text{cpt},k}$  for notional simplicity.

## III. PROBLEM FORMULATION

### A. Performance Metric of Tile Prediction

Average segment degree of overlap (average-DoO) has been used to measure the prediction performance for a VR video [8]. It indicates the average overlap of the predicted tiles and the requested tiles among all the proactively streamed segments, which is defined as

$$\mathcal{D}(t_{\text{obw}}) \triangleq \frac{1}{L - l_0 + 1} \sum_{l=l_0}^L \frac{\mathbf{q}_l^\top \cdot \mathbf{e}_l(t_{\text{obw}})}{\|\mathbf{q}_l\|_1} \in [0, 100\%]$$

where  $\mathbf{q}_l \triangleq [q_{l,1}, \dots, q_{l,M}]^\top$  denotes the ground-truth of the tile requests for the segment with  $q_{l,m} \in \{0, 1\}$ ,  $\mathbf{e}_l(t_{\text{obw}}) \triangleq [e_{l,1}(t_{\text{obw}}), \dots, e_{l,M}(t_{\text{obw}})]^\top$  denotes the predicted tile requests for the segment with  $e_{l,m}(t_{\text{obw}}) \in \{0, 1\}$ ,  $(\cdot)^\top$  denotes transpose of a vector, and  $\|\cdot\|_1$  denotes the  $\ell_1$  norm of a vector. When the  $m$ th tile in the  $l$ th segment is truly requested,  $q_{l,m} = 1$ , otherwise  $q_{l,m} = 0$ . When the tile is predicted to be requested,  $e_{l,m}(t_{\text{obw}}) = 1$ , otherwise it is zero. We consider  $\|\mathbf{e}_l(t_{\text{obw}})\|_1 = N_{\text{fov}}$ . A larger value of average-DoO indicates a better prediction.

As the verified Assumption 1 in [8] states, a predictor can be more accurate with a longer observation window. Therefore, average-DoO is a monotonically increasing function of  $t_{\text{obw}}$ .

### B. Communication and Computing Capability as well as Resources Rate

The capability of communication and computing (CC) can be used to measure the capability of streaming tiles. It is the ratio of tiles in a segment that can be rendered and transmitted with assigned transmission and computing rates and corresponding durations, i.e.,

$$C_{\text{cc}}(t_{\text{com}}, t_{\text{cpt}}) \triangleq \min \left\{ \frac{C_{\text{com}} t_{\text{com}}}{s_{\text{com}}}, \frac{C_{\text{cpt}} t_{\text{cpt}}}{s_{\text{cpt}}}, M \right\} / M$$

where  $\min \left\{ \frac{C_{\text{com}} t_{\text{com}}}{s_{\text{com}}}, \frac{C_{\text{cpt}} t_{\text{cpt}}}{s_{\text{cpt}}}, M \right\}$  is the number of tiles that can be computed and transmitted,  $s_{\text{com}} = p x_w \cdot p x_h \cdot b \cdot r_f \cdot T_{\text{seg}} / \gamma_c$  [1] is the number of bits in each tile for transmission,  $s_{\text{cpt}} = p x_w \cdot p x_h \cdot b \cdot r_f \cdot T_{\text{seg}}$  is the number of bits in a tile for rendering,  $p x_w$  and  $p x_h$  are the pixels in wide and high of a tile,  $b$  is the number of bits per pixel relevant to color depth [1],  $r_f$  is the frame rate, and  $\gamma_c$  is the compression ratio.

To reflect the capability of streaming tiles in unit time, we further define the *resources rate* as

$$R_{cc} \triangleq \frac{C_{cc}(t_{com}, t_{cpt})}{t_{cc}}, \quad (3)$$

### C. Metric of Privacy-aware Quality of Experience

For proactive tile-based streaming without privacy requirement, the QoE can be measured by the percentage of the correctly streamed tiles among all the requested tiles [8]. When considering the spatial degree of privacy, we should also consider whether the sDoP can be satisfied. This is because if the QoE is only captured by the percentage of the correctly predicted tiles, then, the MEC server can still obtain the accurate location of requested tiles from the feedback of QoE from the HMD. Therefore, the privacy-aware QoE should consist of two parts: (1) The percentage of correctly streamed tiles. (2) The level of sDoP satisfaction. For arbitrary given predictor, sDoP, and resources, we consider the following privacy-aware QoE metric

$$QoE \triangleq \frac{1}{L - l_0 + 1} \sum_{l=l_0}^L \underbrace{\frac{(\mathbf{q}_l)^T \cdot \mathbf{s}_l}{\|\mathbf{q}_l\|_1}}_{\text{percent of correctly streamed tiles}} \cdot \underbrace{\frac{(\mathbf{q}_l^p)^T \cdot \mathbf{s}_l}{\|\mathbf{q}_l^p\|_1}}_{\text{sDoP satisfaction}}$$

where  $\mathbf{s}_l \triangleq [s_{l,1}, \dots, s_{l,M}]^T$  denotes the selected tiles for streaming with  $s_{l,m} \in \{0, 1\}$ ,  $\mathbf{q}_l \triangleq [q_{l,1}^p, \dots, q_{l,M}^p]^T$  denotes a mixture of real and camouflaged tile requests for the segment with  $q_{l,m}^p \in \{0, 1\}$ . When the tiles are selected,  $s_{l,m} = 1$ , otherwise  $s_{l,m} = 0$ . When the tile is requested,  $q_{l,m}^p = 1$ , otherwise  $q_{l,m}^p = 0$ . The number of selected tiles is limited by the CC capability, i.e.,  $\|\mathbf{s}_l\|_1 = C_{cc}(t_{com}, t_{cpt}) \cdot M$ . The number of privacy-protected requested tiles depends on sDoP, i.e.,  $\|\mathbf{q}_l^p\|_1 = N_p(\rho_s)$ .

To gain useful insight, we assume that the selected tiles are the mixture of real and camouflaged tile requests, i.e.,  $\mathbf{s}_l = \mathbf{q}_l^p$ . Hence the number of selected tiles and privacy-protected tiles are also identical, i.e.,

$$C_{cc}(t_{com}, t_{cpt}) \cdot M = N_p(\rho_s) \quad (4)$$

Then, the privacy-aware QoE degenerates into

$$QoE = \frac{1}{L - l_0 + 1} \sum_{l=l_0}^L \frac{(\mathbf{q}_l)^T \cdot \mathbf{q}_l^p}{\|\mathbf{q}_l\|_1} \quad (5)$$

We can observe that the QoE is affected by the average-DoO and the CC capability, which can be expressed as

$$QoE = \mathcal{Q}(\mathcal{D}(t_{obw}), C_{cc}(t_{com}, t_{cpt})) \in [0, 100\%]$$

When the value of the QoE is 100%, all the truly requested tiles in a VR video are proactively computed and delivered before playback. Moreover, the MEC server only obtains the mixture of real and camouflaged tile requests.

Since the average-DoO is a monotonically increasing function of  $t_{obw}$ , and the QoE is the monotonically increasing function of  $\mathcal{D}(t_{obw})$ . Then, we have the following remark:

**Remark 1:** The privacy-aware QoE monotonically increases with  $t_{obw}$ .

## IV. SDOP: CONTRADICTION ROLES FOR THE QOE

In this section, we investigate the role of sDoP for the privacy-aware QoE. To this end, we first optimize durations for observation window, communication, and computing to maximize QoE. From the obtained closed-form solution, we investigate the impact of sDoP on average-DoO and CC capability, respectively. Finally, we discuss the overall impact of sDoP on the QoE.

### A. Joint Optimization of the Durations for Prediction, Communication, and Computing

Given arbitrary computing rate  $C_{cpt}$ , transmission rate  $C_{com}$  and sDoP  $\rho_s$ , we aim to find the optimal durations for observation window, communication and computing to achieve maximized QoE, i.e.,

$$\mathbf{P0} : \max_{t_{obw}, t_{cpt}, t_{com}} \mathcal{Q}(\mathcal{D}(t_{obw}), C_{cc}(t_{com}, t_{cpt})) \quad (6a)$$

$$s.t. \quad C_{cc}(t_{com}, t_{cpt}) = \frac{N_p(\rho_s)}{M} \quad (6b)$$

$$t_{obw} + t_{cpt} + t_{com} = T_{ps} \quad (6c)$$

As derived in the Appendix, the solution of **P0** is,

$$t_{obw}^* = \left\lfloor \left( T_{ps} - \left( \frac{s_{com}}{C_{com}} + \frac{s_{cpt}}{C_{cpt}} \right) \cdot N_p(\rho_s) \right) / \tau \right\rfloor \quad (7a)$$

$$t_{com}^* = \frac{s_{com} N_p(\rho_s)}{C_{com}} \quad t_{cpt}^* = \frac{s_{cpt} N_p(\rho_s)}{C_{cpt}} \quad (7b)$$

where  $\tau$  (in seconds) is the sampling interval of the user behavior-related data in the observation window. The optimal duration for communication and computing  $t_{cc}^*$  can be obtained from (7b) as

$$t_{cc}^* = \left( \frac{s_{com}}{C_{com}} + \frac{s_{cpt}}{C_{cpt}} \right) \cdot N_p(\rho_s) \quad (8)$$

By substituting (7b) into (3), the maximized resources rate is

$$R_{cc}^* = 1 / \left( \frac{s_{com} M}{C_{com}} + \frac{s_{cpt} M}{C_{cpt}} \right) \quad (9)$$

where  $\left( \frac{s_{com} M}{C_{com}} + \frac{s_{cpt} M}{C_{cpt}} \right)$  is the required optimal duration to render and transmit all of  $M$  tiles in a segment. By substituting (9) into (7a),  $t_{obw}^*$  can also be expressed as

$$t_{obw}^* = \left\lfloor \left( T_{ps} - \frac{N_p(\rho_s)}{R_{cc}^* \cdot M} \right) / \tau \right\rfloor \quad (10)$$

### B. Contradictory Roles of sDoP

1) *Improve the CC Capability:* By substituting (8) and (9) into (3), the CC capability can be rewritten as follows:

$$C_{cc}(t_{com}^*, t_{cpt}^*) = R_{cc}^* t_{cc}^*,$$

Further considering (8) and (9), we can find that the resource rate  $R_{cc}^*$  has no relation with  $\rho_s$ . Besides, the optimal total duration for communication and computing  $t_{cc}^*$  increases with  $\rho_s$ . This means that the increase of  $\rho_s$  improves the CC capability.

2) *Degrade the Average-DoO*: With the increase of  $\rho_s$ , the duration of observation window  $t_{\text{obw}}^* = T_{\text{ps}} - t_{\text{cc}}^*$  will be reduced, which can also be verified from (7a). The reduction of  $t_{\text{obw}}^*$  degrades the average-DoO.

In Fig. 3, we use the values of  $t_{\text{obw}}^*$  obtained from (7a) to visualize the impact of  $\rho_s$  on the average-DoO. We can observe that as the increase of  $\rho_s$ , the reduction of  $t_{\text{obw}}^*$  is discrete, which comes from the discrete sampling in the observation window. Besides, the value of  $t_{\text{obw}}^*$  increases with the maximized resource rate  $R_{\text{cc}}^*$ . This is because when the resources rate is increased, privacy-protected requested tiles can be streamed with less duration, i.e.,  $t_{\text{cc}}^*$  is reduced. Then,  $t_{\text{obw}}^* = T_{\text{ps}} - t_{\text{cc}}^*$  is increased.

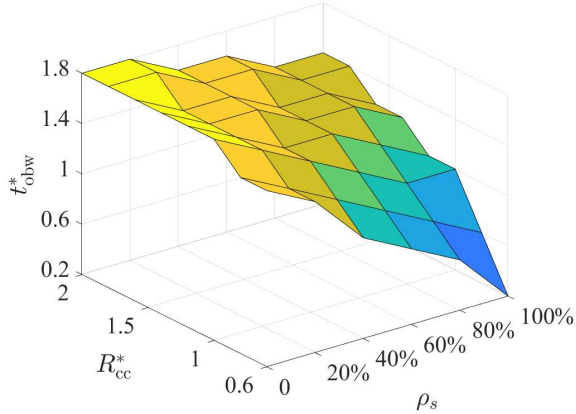


Fig. 3:  $t_{\text{obw}}^*$  v.s.  $R_{\text{cc}}^*$  and  $\rho_s$ .

3) *Overall Impact*: For the final QoE, the impact of sDoP is complicated. On the one hand, it improves the CC capability. On the other hand, it degrades the average-DoO. Generality speaking, the overall effect depends on if the QoE is dominated by the increase of CC capability or the reduction of the average-DoO.

## V. TRACE-DRIVEN NUMERICAL RESULTS

In this section, we show the overall impact of sDoP on QoE via trace-driven numerical results.

First, we consider the prediction task on a real dataset [10], where 300 traces of head movement positions from 30 users watching 10 VR videos are used for training and testing predictors.<sup>1</sup> We randomly split the total traces into training and testing sets with the ratio 8:2.

We use two predictors, *position-only* and *no-motion* predictors, which achieve the state-of-the-art accuracy for the dataset, according to tests in [12]. The *position-only* predictor employs a sequence-to-sequence LSTM-based architecture, which uses the time series of past head movement positions as input, to predict the time series of future positions [12]. The predictor does not consider the time required for computing and communication as well as the spatial degree of privacy. To reserve time for computing and communication, we tailor the predictor as follows. Set the duration between the end of the observation window and the beginning of the prediction windows as  $t_{\text{cc}}^*$ , set the durations of observation and prediction

windows as  $t_{\text{obw}}^*$  and  $T_{\text{seg}}$ , respectively. To satisfy the privacy requirement, we consider a classical federated learning, FederatedAveraging algorithm in [14]. The settings of the federated learning are as follows. For each round, we select *all* of  $K = 30$  users to update the model parameters of the predictor. The number of local epochs for each user is  $E_l = 50$ , the number of communication rounds is  $R = 10$ . Hence, every trace in the train set is used  $50 \times 10 = 500$  times for training, which is consistent with the centralized training [12]. The weight of model parameter of the  $k$ th user among the overall model parameter is  $w_k = \frac{n_k}{N_{\text{train}}}$ , where  $N_{\text{train}} = 300 \times 0.8 = 240$  is the total number of traces in the train set,  $n_k$  is the number of video traces that belong to  $k$ th user in the training set. Due to the random division of training and testing sets,  $n_k$  varies from 6 to 10. We refer to the predictor as *tailored federated position-only* predictor. Other details and hyper-parameters of the tailored predictor are the same as the *position-only* predictor [12]. The *no-motion* predictor simply uses the last position in the observation window as the predicted time series of future positions [12].

The playback duration of a segment is set as  $T_{\text{seg}} = 1$  s [15]. We consider  $T_{\text{ps}} = 2T_{\text{seg}} = 2$  s. Each segment is divided into  $M = 200$  tiles in 10 rows and 20 columns [10]. We consider the VR video with  $3840 \times 2160$  pixels [15] and  $b = 12$  bits per pixel [1]. Then, the pixels in wide and high of a tile are respectively  $px_w = 3840/20 = 192$  and  $px_h = 2160/10 = 216$ . The frame rate of VR video is  $r_f = 30$  frames per second [15]. The compression ratio is  $\gamma_c = 2.41$  [16]. The number of bits in each tile for transmission and rendering can be calculated as  $s_{\text{com}} = px_w \cdot px_h \cdot b \cdot r_f \cdot T_{\text{seg}} / \gamma_c = 5.9$  Mbits and  $s_{\text{cpt}} = px_w \cdot px_h \cdot b \cdot r_f \cdot T_{\text{seg}} = 14.2$  Mbits, respectively.

The maximized resources rate  $R_{\text{cc}}^*$  depends on the configured communication and computing resources as well as the number of users. For example, when  $K = 4$ ,  $N_t = 8$ ,  $P = 24$  dBm,  $B = 150$  MHz, and  $d_k = 5$  m, the ensemble-average transmission rate for a user is  $C_{\text{com}} = 2.85$  Gbps [8]. When Nvidia RTX 8000 GPU is used for rendering VR videos for four users, the computing rate for a user is  $C_{\text{cpt}} = 2.2$  Gbps [8]. Then, the maximized resources rate is  $R_{\text{cc}}^* = 1 / \left( \frac{s_{\text{com}} M}{C_{\text{com}}} + \frac{s_{\text{cpt}} M}{C_{\text{cpt}}} \right) = 0.6$ . To reflect the variation of configured resources, we set  $R_{\text{cc}}^* \in [0.6, 2]$ .

The size of FoVs are modeled by  $100^\circ \times 100^\circ$  circles [12], [17]. According to our tests, the average number of tiles in a FoV is  $N_{\text{fov}} = 33$ . To gain useful insight, we assume that all users have identical sDoP requirement among all videos, ranging from 0 to 100%. Given sDoP  $\rho_s$  and maximized resource rates  $R_{\text{cc}}^*$ , the optimal duration of observation window  $t_{\text{obw}}^*$  can be obtained from (10). Then, given  $t_{\text{obw}}^*$  and two predictors, the predicted time series of positions can be obtained. Given sDoP, the CC capability can be obtained from (4). Then, given the CC capability and the predicted time series of positions, the privacy-protected requested tiles can be determined by scheme (b) of section IV-C in [4]. Finally, the QoE is first calculated from (5), and then averaged over the testing set.

In Fig. 4, we show the average QoE achieved by two predictors versus the assigned resources rate and sDoP. We

<sup>1</sup>The original dataset contains the traces of 50 users. According to the analysis in [12], [13], the traces of the first 20 users may have some mistakes, thus we only use the traces of the other 30 users.

can observe that no matter how much the resources rate is assigned, which predictor is employed, the average QoE can always be improved with the increase of  $\rho_s$ . Besides, **The increase of  $\rho_s$  is equivalent to the increase of assigned resources rate in terms of improving the QoE.** For example, consider the point ‘‘P’’ in Fig. 4b. To achieve QoE = 94%, increasing the sDoP by 0.2 is equivalent to increasing  $R_{cc}^*$  by 1.4.

To further understand how the QoE is affected by the sDoP, we consider a case where the resource rates  $R_{cc}^* = 0.6$  as an example, to investigate how the CC capability  $C_{cc}(t_{com}^*, t_{cpt}^*)$ , average-DoO  $\mathcal{D}(t_{obw}^*)$ , and average QoE is affected by  $\rho_s$ . As shown in Fig. 5, for both predictors, the increase of sDoP improves the CC capability  $C_{cc}(t_{com}^*, t_{cpt}^*)$  and degrades average-DoO  $\mathcal{D}(t_{obw}^*)$ . Since the degradation of average-DoO is relative small, the QoE is dominated by the increase of the CC capability.

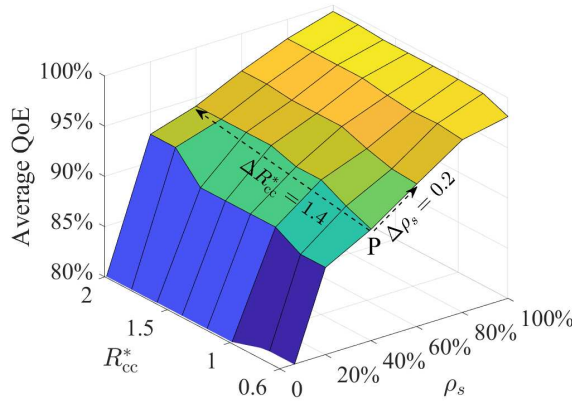
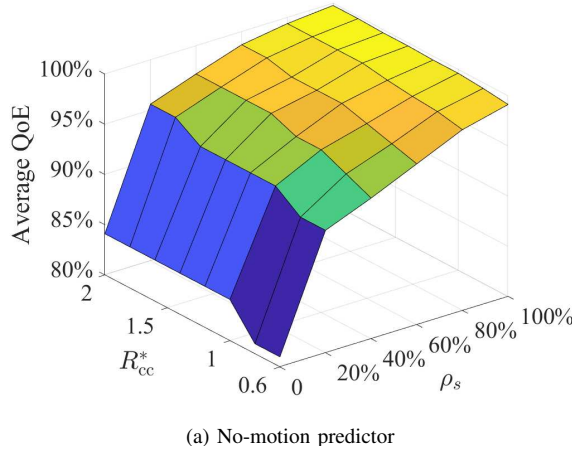


Fig. 4: Average QoE v.s. resource rates and sDoP.

## VI. CONCLUSION

In this paper, we defined spatial privacy requirement for better privacy protection and investigated the impact of spatial privacy requirement on the VR video streaming. By duration optimization and analyzing of the obtained optimal closed-form solution, we found the relation between sDoP and QoE. The analysis showed that the increase of sDoP improves the CC capability but degrades the average-DoO. The overall impact depends on which factor dominates the QoE. Simulation

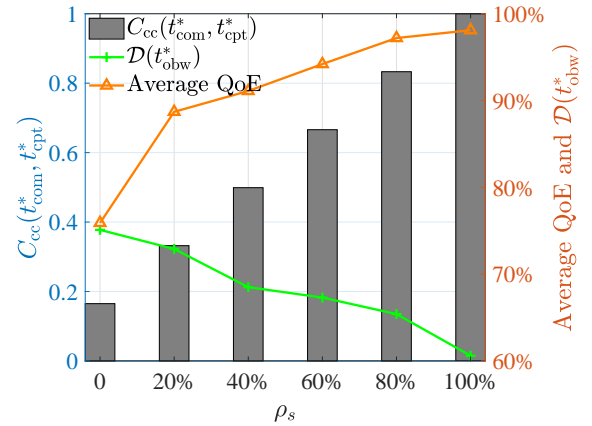
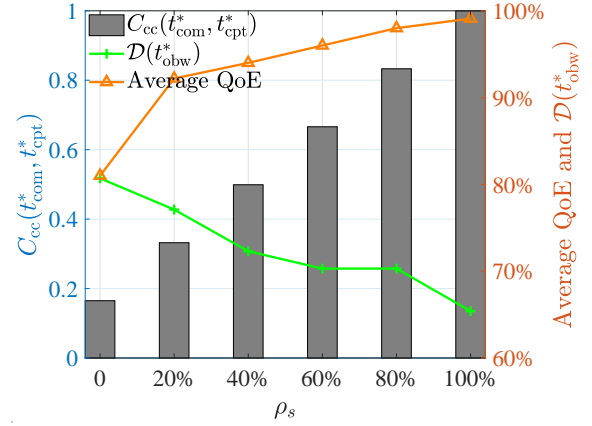


Fig. 5: Average QoE, CC capability, and average-DoO v.s. sDoP,  $R_{cc}^* = 0.6$ .

with two predictors on a real dataset validated the analysis and showed that the overall impact of sDoP is to improve the QoE.

## APPENDIX A

### PROOF OF THE SOLUTION OF PROBLEM P0

We can observe that for arbitrary  $\rho_s$ , CC capability is fixed as  $C_{cc}(t_{com}, t_{cpt}) = \frac{N_p(\rho_s)}{M}$ . Then, QoE becomes a function of a single variable  $\mathcal{D}(t_{obw})$ . Furthering consider **Remark 1**, we can find maximizing  $\mathcal{D}(t_{obw})$  is equivalent to maximize  $t_{obw} = T_{ps} - (t_{com} + t_{cpt})$ . Then, without loss of optimality, **P0** can be transformed as

$$\min_{t_{cpt}, t_{com}} t_{com} + t_{cpt} \quad (11a)$$

$$s.t. \quad \min \left\{ \frac{C_{com}t_{com}}{s_{com}}, \frac{C_{cpt}t_{cpt}}{s_{cpt}}, M \right\} = N_p(\rho_s), \quad (11b)$$

where (11b) can be obtained by multiplying both sides of (6b) by  $M$ . Since  $N_p(\rho_s) \leq M$ , (11b) can be further simplified as  $\left\{ \frac{C_{com}t_{com}}{s_{com}}, \frac{C_{cpt}t_{cpt}}{s_{cpt}} \right\} = N_p(\rho_s)$ . According to the constraint, we discuss problem (11) in the following three cases.

(1) When  $\frac{C_{com}t_{com}}{s_{com}} > \frac{C_{cpt}t_{cpt}}{s_{cpt}}$ , upon substituting into (11b), we have  $t_{cpt} = \frac{N_p(\rho_s)s_{cpt}}{C_{cpt}}$ . Upon substituting into the condition  $\frac{C_{com}t_{com}}{s_{com}} > \frac{C_{cpt}t_{cpt}}{s_{cpt}}$ , we obtain  $t_{com} \geq \frac{N_p(\rho_s)s_{com}}{C_{com}}$ . Then, we obtain  $t_{com} + t_{cpt} > \frac{s_{com}N_p(\rho_s)}{C_{com}} + \frac{s_{cpt}N_p(\rho_s)}{C_{cpt}}$ .

(2) When  $\frac{C_{com}t_{com}}{s_{com}} < \frac{C_{cpt}t_{cpt}}{s_{cpt}}$ , upon substituting into (11b), we have  $t_{com} = \frac{N_p(\rho_s)s_{com}}{C_{com}}$ . Upon substituting the condition  $\frac{C_{com}t_{com}}{s_{com}} < \frac{C_{cpt}t_{cpt}}{s_{cpt}}$ , we obtain  $t_{cpt} > \frac{N_p(\rho_s)s_{cpt}}{C_{cpt}}$ . Then, we obtain  $t_{com} + t_{cpt} > \frac{s_{com}N_p(\rho_s)}{C_{com}} + \frac{s_{cpt}N_p(\rho_s)}{C_{cpt}}$ .

(3) When  $\frac{C_{com}t_{com}}{s_{com}} = \frac{C_{cpt}t_{cpt}}{s_{cpt}}$ , upon substituting into (11b), we have  $t_{com} = \frac{N_p(\rho_s)s_{com}}{C_{com}}$  and  $t_{cpt} = \frac{N_p(\rho_s)s_{cpt}}{C_{cpt}}$ . Then, we obtain  $t_{com} + t_{cpt} = \frac{s_{com}N_p(\rho_s)}{C_{com}} + \frac{s_{cpt}N_p(\rho_s)}{C_{cpt}}$ .

From the three cases, we obtain the solution as  $t_{com}^* = \frac{s_{com}N_p(\rho_s)}{C_{com}}$ ,  $t_{cpt}^* = \frac{s_{cpt}N_p(\rho_s)}{C_{cpt}}$ . Upon substituting into (6c),  $t_{obw}$  can be obtained as  $t_{obw} = T_{ps} - \left( \frac{s_{com}}{C_{com}} + \frac{s_{cpt}}{C_{cpt}} \right) \cdot N_p(\rho_s)$ . Note that although the duration of the observation window can be continuous, the user behavior-related data is sampled discretely. Then, the efficient duration of the observation window is

$$t_{obw}^* = \left\lfloor \left( T_{ps} - \left( \frac{s_{com}}{C_{com}} + \frac{s_{cpt}}{C_{cpt}} \right) \cdot N_p(\rho_s) \right) / \tau \right\rfloor \quad (12)$$

## REFERENCES

- [1] iLab, “Cloud VR network solution whitepaper,” Huawei Technologies CO., LTD., Tech. Rep., 2018. [Online]. Available: [https://www.huawei.com/minisite/pdf/ilab/cloud\\_vr\\_network\\_solution\\_white\\_paper\\_en.pdf](https://www.huawei.com/minisite/pdf/ilab/cloud_vr_network_solution_white_paper_en.pdf)
- [2] F. Qian, L. Ji, B. Han, and V. Gopalakrishnan, “Optimizing 360 video delivery over cellular networks,” *ACM SIGCOMM Workshop*, 2015.
- [3] M. R. Miller, F. Herrera, H. Jun, J. A. Landay, and J. N. Bailenson, “Personal identifiability of user tracking data during observation of 360-degree VR video,” *Scientific Reports*, vol. 10, no. 1, pp. 1–10, 2020.
- [4] X. Wei and C. Yang, “Privacy-aware VR streaming,” *arXiv:2104.09779*, 2021.
- [5] B. David-John, D. Hosfelt, K. Butler, and E. Jain, “A privacy-preserving approach to streaming eye-tracking data,” *IEEE Transactions on Visualization and Computer Graphics*, vol. 27, no. 5, p. 2555–2565, May 2021. [Online]. Available: <http://dx.doi.org/10.1109/TVCG.2021.3067787>
- [6] C.-L. Fan, W.-C. Lo, Y.-T. Pai, and C.-H. Hsu, “A survey on 360° video streaming: Acquisition, transmission, and display,” *ACM Comput. Surv.*, vol. 52, no. 4, Aug. 2019.
- [7] 3GPP, “Extended reality (XR) in 5G,” 2020, 3GPP TR 26.928 version 16.0.0 release 16.
- [8] X. Wei, C. Yang, and S. Han, “Prediction, communication, and computing duration optimization for VR video streaming,” *IEEE Trans. Commun.*, vol. 69, no. 3, pp. 1947–1959, 2021.
- [9] C. Perfecto, M. S. Elbamy, J. Del Ser, and M. Bennis, “Taming the latency in multi-user VR 360°: A QoE-aware deep learning-aided multicast framework,” *IEEE Trans. Commun.*, vol. 68, no. 4, pp. 2491–2508, 2020.
- [10] W.-C. Lo, C.-L. Fan, J. Lee, C.-Y. Huang, K.-T. Chen, and C.-H. Hsu, “360° video viewing dataset in head-mounted virtual reality,” *ACM MMSys*, 2017.
- [11] D. Bethanabhotla, G. Caire, and M. J. Neely, “Adaptive video streaming for wireless networks with multiple users and helpers,” *IEEE Trans. Commun.*, vol. 63, no. 1, pp. 268–285, 2015.
- [12] Miguel Romero, “Analysis of head motion prediction in virtual reality,” <https://gitlab.com/miguelfromeror/head-motion-prediction/tree/master/>.
- [13] M. F. R. Rondón, L. Sassatelli, R. Aparicio-Pardo, and F. Precioso, “A unified evaluation framework for head motion prediction methods in 360° videos,” *ACM MMSys*, 2020.
- [14] B. McMahan, E. Moore, D. Ramage, S. Hampson, and B. A. y Arcas, “Communication-efficient learning of deep networks from decentralized data,” *PMLR AISTATS*, 2017.
- [15] A. Mahzari, A. T. Nasrabadi, A. Samiei, and R. Prakash, “FoV-aware edge caching for adaptive 360° video streaming,” *ACM MM*, 2018.
- [16] M. Zhou, W. Gao, M. Jiang, and H. Yu, “HEVC lossless coding and improvements,” *IEEE Trans. Circuits Syst. Video Technol.*, vol. 22, no. 12, pp. 1839–1843, 2012.
- [17] C.-L. Fan, J. Lee, W.-C. Lo, C.-Y. Huang, K.-T. Chen, and C.-H. Hsu, “Fixation prediction for 360° video streaming in head-mounted virtual reality,” *ACM NOSSDAY*, 2017.